

MIT Open Access Articles

An Implantable MEMS Drug Delivery Device for Rapid Delivery in Ambulatory Emergency Care

The MIT Faculty has made this article openly available. **Please share** how this access benefits you. Your story matters.

Citation: N. Elman, H. Ho Duc, and M. Cima, "An implantable MEMS drug delivery device for rapid delivery in ambulatory emergency care," *Biomedical Microdevices*, vol. 11, Jun. 2009, pp. 625-631.

As Published: <http://dx.doi.org/10.1007/s10544-008-9272-6>

Publisher: Springer Netherlands

Persistent URL: <http://hdl.handle.net/1721.1/49478>

Version: Author's final manuscript: final author's manuscript post peer review, without publisher's formatting or copy editing

Terms of use: Article is made available in accordance with the publisher's policy and may be subject to US copyright law. Please refer to the publisher's site for terms of use.



An Implantable MEMS Drug Delivery Device for Rapid Delivery in Ambulatory Emergency Care

N. M. Elman, H. L. Ho Duc, M. J. Cima

Massachusetts Institute of Technology, Department of Materials Science and Engineering
77 Massachusetts Ave, 12-011, Cambridge, MA, USA, 02139

*Corresponding author: Noel M. Elman, nelman@mit.edu

Abstract

We introduce the first implantable drug delivery system based on MEMS (Micro-Electro-Mechanical-Systems) technology specifically designed as a platform for treatment in ambulatory emergency care. The device is named IRD³ (implantable rapid drug delivery device) and allows rapid delivery of drugs. Vasopressin was used as a model drug for *in vitro* tests as it is a commonly used drug for cardiac resuscitation. Experimental results reveal that the IRD³ provides an effective method for rapid delivery without significant drug degradation. Several medical uses and delivery modalities for IRD³ are proposed.

1. Introduction

Implantable drug delivery devices have demonstrated their great potential in a vast number of applications for which the controlled and accurate delivery of critically prescribed drug doses is required without direct medical intervention. A variety of implantable devices based on Micro-Electro-Mechanical-Systems (MEMS) technology has already been demonstrated for chronic illnesses (Prescott, et al. 2006). These devices also show great potential for treatment of a number of pathologies in emergency situations without the assistance of a physician or medical practitioner.

Actively controlled devices provide advantages over passive release devices, as the drug delivery process can be controlled actively after implantation and even engaged

telemetrically, as opposed to passive devices that depend on the degradation chemistry of the specific device materials in the intended implantation region. Active devices based on MEMS technology have been previously investigated and proven successful for *in vivo* use in multiple clinical applications. Such active devices are based on MEMS technology, such as micro-pumps (Nguyen, et al. 2002), electro-chemical or electrical degradation of membranes for multiple-reservoir drug delivery chips (Santini, et al. 1999; Grayson, et al. 2003).

MEMS technology allowed the successful miniaturization of micro-pumps for drug delivery, providing for active delivery of fluids from single or multiple reservoirs. The low delivery rates, low reliability due to the dependence on mechanical moving parts in fluids, and high power consumption are among the prime limitations of an implantable drug delivery device that relies on micro-pumps. Drug delivery devices characterized by multiple-reservoir architectures and based on electrical actuation mechanisms provide a more reliable platform. These devices typically can also rely on electro-thermal actuation to rupture a reservoir sealing membrane as a result of an applied electrical potential, allowing the drugs inside of reservoirs to freely diffuse into the region of interest (Maloney, et al. 2005; Grayson, et al. 2005).

A number of implantable drug delivery devices have been investigated for use in chronic and non-chronic diseases in ambulatory settings without medical intervention, such as cancer, diabetes, and osteoporosis (Staples, et al. 2006). These implantable devices provide a significant improvement in the bioavailability of drugs, but their use is mainly limited to treatment of chronic illnesses as they rely on diffusion and small delivery volumes, with complete release achieved in a few hours. Current implantable

drug delivery devices based on MEMS technology are therefore not adequate as a solution for immediate treatment of illnesses in trauma care. None of the currently available technologies for implantable drug delivery devices fulfill the requirements for rapid *in vivo* treatment of pathologies in emergency care situations. The challenge lies in the implementation of an active drug delivery device capable of storing large volumes, preferably without any moving parts to increase performance reliability, and mainly characterized by high delivery rates to achieve treatment in a few minutes as opposed to a few hours. The development of implantable devices for emergency treatments that require rapid and reliable drug delivery is thus the main motivation of this research work.

We present the first rapid drug delivery platform suitable for implementation as a smart micro-implant for high-risk patients. This novel device can be useful for a number of delivery modalities, including subcutaneous, intraperitoneal, intramuscular, and transdermal delivery. Potential pathologies that the device can address with patients at high risk include: cardiac arrest, vasovagal syncope, angina, strokes, allergy, and epilepsy. The premise is to use the device to provide a drug bolus upon triggering caused by the detection of specific symptoms. The device has been implemented for subcutaneous use, and vasopressin has been chosen as a model drug since it is commonly used for a number of cardiac applications. The micro-implants have been named IRD³ (Implantable Rapid Drug Delivery Device). The IRD³ can also be implemented to communicate and work as an add-on with current cardiac devices, such as pacemakers and defibrillators. We believe that the ramifications of the IRD³ can be applied to a wide variety of medical applications that require immediate care of high-risk patients.

2. Device Architecture

The modular device architecture is shown in Figure 1 and is comprised of three layers: a large single reservoir layer, where the drug solution is stored; a membrane layer that hermetically seals the drug reservoir, and from where the drug is ejected; and an actuation layer, where bubbles are formed. All materials of construction of this device (silicon, silicon nitride, silicon dioxide, gold and titanium) have been shown to be biocompatible (Kotzar et al, 2002; Voskerician et al, 2003). The actuation layer is defined by micro-resistors, which once activated, rapidly and locally heat the contained fluid to generate bubbles. The increase in pressure caused by the bubbles ruptures the membrane and jets the contained solution out of the device, allowing the delivery of 20 μl in 45 seconds. The device operational design and principles are introduced, followed by a description of the fabrication process and experimental validation of the device to address its performance characteristics.

3. Device Design

Bubble nucleation achieved by heating a liquid is a well-known phenomenon, and it can be initiated by electrically heating a resistive element to generate localized boiling. The sudden increase in pressure bursts the sealing membranes, thereby releasing the drugs at a high rate. The design of the actuation layer is therefore critical for the performance of the device. The actuation layer consists of three resistive elements that were optimized to maximize heat transfer into a localized fluid volume. The resistor area was designed to be compact in order to localize the heat transfer. The power density was designed to reach approximately 25 W/mm^2 in order to exceed the nucleate boiling

threshold and enter the film boiling regime for water (van Stralen, Cole, 1979). Film boiling is desired in order to insulate the bulk of the drug solution from the resistor surface, and prevent drug degradation due to heating. Titanium was chosen as material for the resistive element because it is bio-compatible and characterized by a relatively high resistivity for metals. In order to achieve film boiling, the approximate theoretical resistor was 40 ohms, with dimensions 38 μm wide, 385 μm long, and 120 nm thick, the resistivity of Ti being $4.7 \times 10^{-7} \Omega\text{-m}$. Three resistors of 30 ohms were designed to connect in parallel to achieve a 10-ohm electrical resistance adequate for high-rate delivery. The thickness was optimized to achieve the desired resistor values in order to compensate for impurities in the Ti due to the deposition process. This step involved deposition of several thicknesses of Ti (200 nm, 250 nm, 300 nm, 400 nm) and subsequent measurements of sheet resistance using a four point probe (Keithley SCS-4200, Keithley Instruments Inc., USA). The resultant thickness was 250 nm, providing a sheet resistance of $2.7 \Omega/\square$.

The membrane layer consists of a free-standing silicon nitride membrane that acts as a hermetic seal preventing both the drug inside of the reservoir to diffuse out, and any foreign substance to penetrate inside of the reservoir. Silicon nitride was chosen as the membrane material due to its high density and use as a diffusion-stop layer. Its mechanical properties allow limited elastic deformation while maintaining a hermetic seal. The membrane shatters into micron and submicron fragments as it subjected to a critical pressure. The membrane dimensions were optimized to withstand external pressure and stresses involved in the handling and implantation of the device, but also to allow the membrane to burst when activation of the device increases pressure inside the

device. A design based on a square membrane was chosen for its simplicity in implementation. A finite element analysis (FEA) was performed to simulate the maximum allowed pressure on the membranes. The FEA tool (Cosmos, SolidWorks, Inc., USA) was used to simulate the failure points based on applied pressures for different membrane lateral dimensions, keeping the thickness to a constant 200 nm, and maintaining an overall factor of safety value of above 1, defined as the ratio of the breaking stress of a structure to the estimated maximum stress. Successive differential pressure values were simulated across the surface area of the structure while the resultant minimum safety factor was subsequently monitored. Summary of such simulations can be found in the Electronic Supplementary Material. The results of the simulation revealed that a 400- μm square membrane can withstand differential pressures of up to 5kPa, while maintaining a factor of safety just above minimum value of 1.0, at which point the membrane material is no longer elastic and just starts to yield.

Calculations based on standard analytical solutions (Maier-Schneider, 1995) also reveal that the chosen membrane dimensions are structurally robust for this application. Furthermore, the fabricated membranes were tested using a one meter drop test, showing that the membranes are robust for implantation.

4. Fabrication Process

The device fabrication is comprised of three separate processes: the membrane layer, the reservoir layer, and the actuation layer. These processes are independent due to the modular architecture of the device, as was shown in Figure 1. The process for fabrication of these separate layers referred hereinafter is described in Figures 2-3.

The membrane layer was fabricated using micro-machining technology, and comprised of an array of standing SiN membranes is combined with patterned gold fuses, which are designed to act as sensors. A fuse is broken when a membrane is burst, resulting in an open circuit which can be detected by measuring resistance across the fuse. The actuation layer was also fabricated using micro-machining technology on 100-mm SCS substrates. The reservoir layer was 2.25 mm thick Pyrex 7740 wafers, which were drilled to define the reservoir and subsequently diced. Specific details pertaining to the fabrication processes can be found in the Electronic Supplementary Material. The final packaged device is shown in Fig. 4.

5. Experimental Methods and Results

Three sets of experiments were conducted to characterize the device performance. The first experiment consisted of electrical characterization of the device *in vitro* by releasing a dye. Such test was critical to empirically determine the power consumption of the device and qualitatively determine the release rates. The second experiment consisted of quantitatively determining the release rates using radio-labeled vasopressin. The third experiment consisted of quantitatively determining the effects of the actuation mechanism (localized bubble nucleation) on drug degradation using high-pressure liquid chromatography (HPLC).

5.1 Electrical Characterization

The devices were first tested *in vitro* by releasing methylene blue to determine the I-V curve characteristics while optically recording the release event. The devices were placed inside of a 10-ml beaker filled with DI water. An increasing dc-voltage was

applied to the heating elements using a voltage source, as the electrical current was measured. The device was optically inspected and recorded using a video camera connected to a stereoscope in order to register the conditions in which the dye was delivered. Figure 5 shows the I-V curve of the heating elements. The red circle indicates that the device is intended for 9-V operation. Bubbles were observed for an applied dc-voltage of 9 V and the measured current was approximately 650 mA. Figure 6 shows the methylene blue jetted into DI water during actuation. The electrical fuses on top of the membranes were also monitored during each activation and were observed to become open-circuited as the membranes burst, proving that it is possible to interrogate the device by means of impedance measurement to check whether the sealing membrane is opened by the device actuation.

5.2 Radioactive Release

Four devices were filled with 20 μL of radiolabeled vassopressin. An additional three controls were injected directly into water to be measured and determine the loading in all devices. The test devices were activated for 45 seconds, and the media was sampled immediately before and after each device activation. Figure 7 shows the measured loading fraction released after each activation. The results indicate that 92.9 ± 0.7 % of the original loading was released by the devices. Additional information about the radioactive release experiments can be found in the Electronic Supplementary Material.

5.3 Vasopressin HPLC Study

The effect of device actuation on the degradation of vasopressin was determined in three devices. The devices were filled with 20 μL of a 25 mg/mL solution of arginine vasopressin and sealed. Another 20 μL of solution was also directly injected into 5 mL of DI water as control, resulting in a concentration of 0.1 mg/mL. The area fraction of the vasopressin peak for the devices was compared to that of the control, and it was found that $9.0 \pm 0.7\%$ of the vasopressin released by the devices was degraded with respect to the original state of vasopressin injected into the devices, as shown in Figure 8.

Additional information about chromatography experimental methods can be found in the Electronic Supplementary Material.

6. Discussion

The IRD³ is the first implantable device based on MEMS technology that provides a platform for applications requiring rapid drug delivery. The best candidates for the IRD³ are conditions of an urgent nature that would require a bolus shot. We are currently investigating *in vivo* use of this device as a subcutaneous implant to release vasopressin as a model drug. Vasopressin is typically injected intravenously in cardiac resuscitation efforts. Vasopressin is a peptide hormone that can easily be reconstituted, and exhibits thermal stability in water up to 5 days at body temperature, allowing its use in the IRD³ without being significantly affected for a few days. The actuation mechanism of the IRD³ is similar to inkjet printing, as it relies on film boiling, but the volumes of liquid to be displaced are typically 6 orders of magnitude higher. We have optimized the

resistors involved in the bubble nucleation process to guarantee that the nucleation occurs in the film boiling regime. The power density achieved is approximately 25 W/mm^2 allowing an effective increase in the reservoir pressure, while guarantying that the bubble nucleation is deep in the film boiling regime. The electrical characterization showed that activation requires relatively high power, approximately 6 W, for a short period of time of 45 seconds. We envision that this device can be connected to commercially available ultra- high density capacitors, which can easily provide 270 J from a very small size component.

We have demonstrated that the heating involved in the actuation of the device does not significantly affect vasopressin, as the degradation study by RP-HPLC showed. Approximately 91% of the drug was still effective after release. Quantification of device loading fraction released by radiolabeled vasopressin determined that 92.9% of the loaded solution was released in 45 seconds. Hence, approximately 85% of the drug originally loaded into the device is released in its active form. An overhead volume can thus be included when loading the device in order to deliver a consistent target dose.

A potential issue related to the use of this device is the presence of silicon nitride fragments after activation. These fragments exhibit a very limited impact on the surrounding tissue at the moment of membrane bursting. The mass of a $400 \times 400 \times 0.2 \text{ um}$ piece of silicon nitride with a density of 3.4 g/cm^3 is 0.11 ng, which represents a very limited impact on the tissue around the device. The fragments released after activation of the device are not expected to travel from the implantation site, and would eventually be surrounded by a fibrous capsule and isolated from the body. We therefore do not anticipate their presence to be a problem. An alternative solution to the problem is to

implement gold membranes instead of silicon nitride. A gold membrane can be melted by passing a current pulse through it, as has been demonstrated in the past (Maloney, 2005). The limitations of this solution are: the significant increase in current to burst a membrane, and the smaller membrane area required to maintain structural robustness.

The IRD³ can also be used as a complement to current cardiac devices. The device can, for example, be implanted subcutaneously and be connected to an internal pacemaker to treat a number of illnesses such as different forms of syncope (Singer, 1999; Fonarow, et al. 2000; Cavaco, et al. 2003; Sanchez, et al. 2006; Moran, et al. 2006). Potential drug models for this specific application would include atropine or even beta blockers. The IRD³ would work in a closed-loop circuit together with the pacemaker in this case. Another potential use of this device is for treating angina. The IRD³ could be implanted in high-risk patients to deliver vasodilators such as nitrates on demand (Aronow, 2003), without the need to carry pills (typically for sublingual delivery). In this particular case, the application of the IRD³ would be in an open-loop configuration.

Future prospects after this proof of concept include the integration of the device in a wireless platform, to demonstrate remote access and activation for the U.S. Army. This device could be implanted subcutaneously in soldiers exposed to high risk in order to treat hemorrhagic shock in ambulatory settings on the battlefield. Another potential use of this device is for patients who suffer seizures from conditions such as anaphylactic shock for which epinephrine is commonly used; and epilepsy, for which diazepam is typically indicated. We are also investigating the use of the IRD³ to rapidly reconstitute and deliver drugs. This configuration of the device would allow drugs to be implanted for long periods of time, without suffering from thermal degradation, or hydrolyzation. The

drugs would only be reconstituted on demand. The IRD³ could thus be useful in a great number of medical applications where subcutaneous, intramuscular, or transdermal delivery may be required according to the specific situation.

7. Conclusions

The IRD³ represents the first implantable drug delivery device specifically designed to rapidly provide medication. It is a technology platform that can be leveraged for a large number of medical applications. It was shown to provide consistent drug delivery without any major degradation. The IRD³ is an ideal candidate for pathologies that require immediate and ambulatory treatment of high-risk individuals, and allow for rapid and effective treatment. We believe that the ramifications of this technology platform can significantly improve survival rates in ambulatory settings.

8. Acknowledgments

This work was made possible thanks to Army Research Office support via the Institute for Soldier Nanotechnologies (ISN) at MIT (contract: W911NF-07-D-0004). The authors also wish to thank Dustin Rabideau for his assistance during the fabrication process.

10. References

- W. S. Aronow, "Review Article: Treatment of Unstable Angina Pectoris/Non-ST-Segment Elevation Myocardial Infarction in Elderly Patients," *The Journals of Gerontology Series A: Biological Sciences and Medical Sciences*, vol. 58, pp. 927-933, 2003
- D. Cavaco, P. Adragao, C. Aguiar, J. Neves, M. Abecasis, F. Morgado, D. Bonhorst, and R. Seabra-Gomes, "Syncope in implantable cardioverter-defibrillator pacemaker dependent patients," *European Heart Journal*, vol. 23, pp. 665-665, 2002.

- N. M. Elman, S. Krylov, M. Sternheim, Y. Shacham-Diamand, "Multiple aspect-ratio structural integration in single crystal silicon (MASIS) for fabrication of transmissive MOEMS modulators," *Journal of Micro-system Technologies*, Vol. 14, pp. 145-293, 2008
- G. C. Fonarow, Z. Feliciano, N. G. Boyle, L. Knight, M. A. Woo, J. D. Moriguchi, H. Laks, and I. Wiener, "Improved survival in patients with nonischemic advanced heart failure and syncope treated with implantable cardioverter-defibrillator," *American Journal of Cardiology*, vol. 85, pp. 981-985, 2000.
- A. C. R. Grayson, I. S. Choi, B. M. Tyler, P. P. Wang, H. Brem, M. J. Cima, and R. Langer, "Multi-pulse drug delivery from a resorbable polymeric microchip device," *Nature Materials*, vol. 2, pp. 767-772, 2003.
- A. C. R. Grayson, M. J. Cima, and R. Langer, "Size and temperature effects on poly(lactic-co-glycolic acid) degradation and microreservoir device performance," *Biomaterials*, vol. 26, pp. 2137-2145, 2005.
- G. Kotzar, M. Freas, P. Abel, A. Fleischman, S. Roy, C. Zorman, J. M. Moran, and J. Melzak, "Evaluation of MEMS materials of construction for implantable medical devices," *Biomaterials*, vol. 23, pp. 2737-2750, 2002
- D. Maier-Schneider, J. Maibach, E. Obermeier, "A new analytical solution for the load-deflection of square membranes," *Journal of Microelectromechanical Systems*, vol. 4, pp. 238 – 241, 1995
- J. M. Maloney, S. A. Umland, B. F. Polito, N. F. Sheppard, C. M. Pelta, and J. T. Santini, "Electrothermally activated microchips for implantable drug delivery and biosensing," *Journal of Controlled Release*, vol. 109, pp. 244-255, 2005.
- E. G. Moran and L. Mont, "Incidence of syncope after ICD implantation: low or high?," *European Heart Journal*, vol. 27, pp. 2481-2482, 2006.
- N. T. Nguyen, X. Y. Huang, and T. K. Chuan, "MEMS-micropumps: A review," *Journal of Fluids Engineering-Transactions of the Asme*, vol. 124, pp. 384-392, 2002.
- J. H. Prescott, S. Lipka, S. Baldwin, N. F. Sheppard, J. M. Maloney, J. Coppeta, B. Yomtov, M. A. Staples, and J. T. Santini, "Chronic, programmed polypeptide delivery from an implanted, multireservoir microchip device," *Nature Biotechnology*, vol. 24, pp. 437-438, 2006.
- J. M. Sanchez, W. T. Katsiyannis, B. F. Gage, J. Chen, M. N. Faddis, M. J. Gleva, T. W. Smith, and B. D. Lindsay, "Implantable cardioverter-defibrillator therapy improves long-term survival in patients with unexplained syncope, cardiomyopathy, and a negative electrophysiologic study," *Heart Rhythm*, vol. 2, pp. 367-373, 2005.

J. T. Santini, M. J. Cima, and R. Langer, "A controlled-release microchip," *Nature*, vol. 397, pp.335-338, 1999.

J. T. Santini, A. C. Richards, R. Scheidt, M. J. Cima, and R. Langer, "Microchips as controlled drug-delivery devices," *Angewandte Chemie-International Edition*, vol. 39, pp. 2397-2407, 2000.

J. T. Santini, A. C. Richards, R. A. Scheidt, M. J. Cima, and R. S. Langer, "Microchip technology in drug delivery," *Annals of Medicine*, vol. 32, pp. 377-379, 2000.

I. Singer and H. L. Edmonds, "Head-up tilt testing predicts syncope during ventricular tachycardia in implantable cardioverter defibrillator patients," *Journal of Interventional Cardiology*, vol. 11, pp. 205-211, 1998.

M. Staples, K. Daniel, M. J. Cima, and R. Langer, "Application of micro- and nano-electromechanical devices to drug delivery," *Pharmaceutical Research*, vol. 23, pp. 847-863, 2006.

S. van Stralen and R. Cole, *Boiling Phenomena*, vol. 1, ch. 1: Hemisphere Publishing Corporation, 1979.

G. Voskerician, M. S. Shivea, R. S. Shawgo, H. v. Recum, J. M. Anderson, M. J. Cima, and R. Langer, "Biocompatibility and Biofouling of MEMS Drug Delivery Devices," *Biomaterials*, vol. 24, pp. 1959 - 1967, 2003

11. Figures

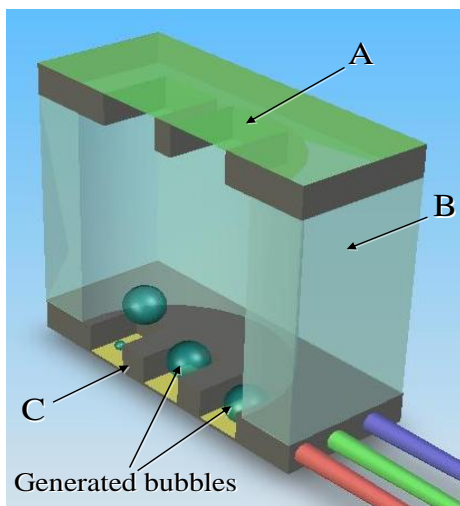


Figure 1: Cross-sectional render of the device showing the three layers: membrane layer (A), reservoir layer (B), actuation layer (C).

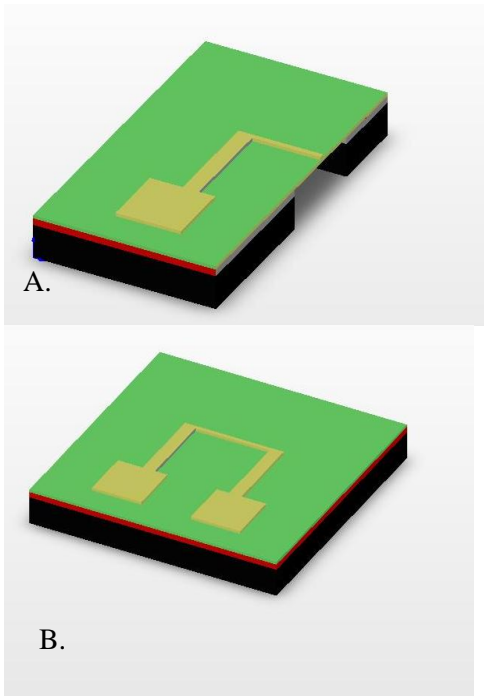


Figure 2: Fabrication sequence for the membrane layer. A. Electrodes on Au, deposited on Si₃N₄ (green), and SiO₂ (red).

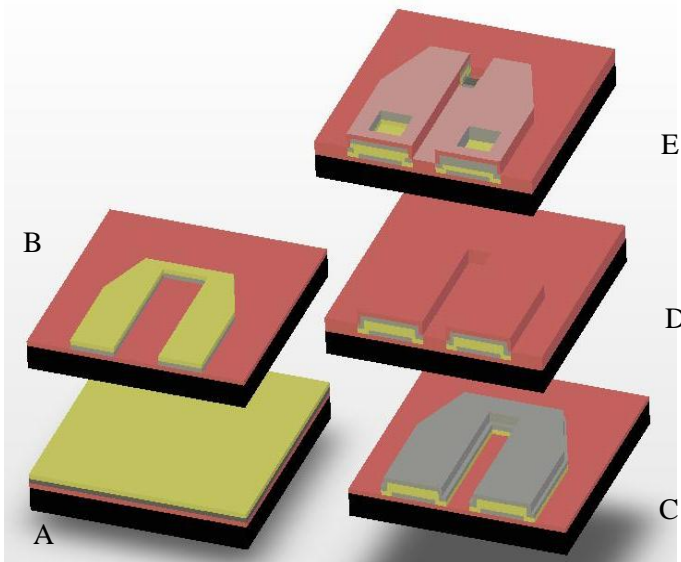


Figure 3: Fabrication of Actuation layer. A. SiO₂, Ti, Au deposition on SCS substrate. B. Definition of electrodes and resistor. C. Ti, Au encapsulation. D. SiO₂ deposition. E. Electrodes vias and exposure of Ti resistor.

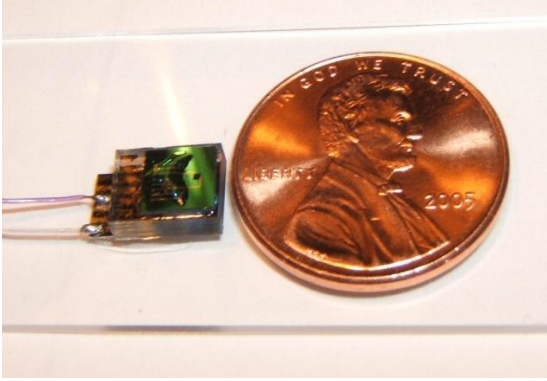


Figure 4: Final packaged device.

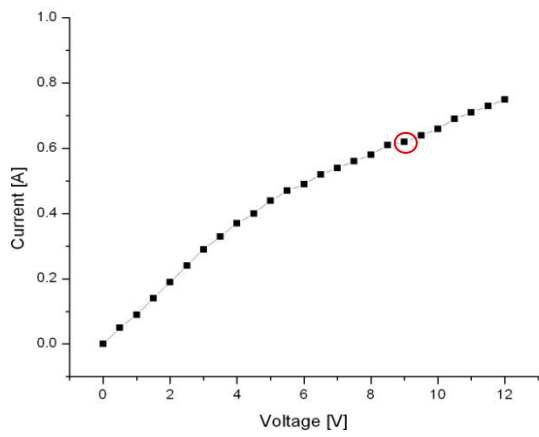


Figure 5: I-V response. The device was designed to be active at 9 V, indicated in red.

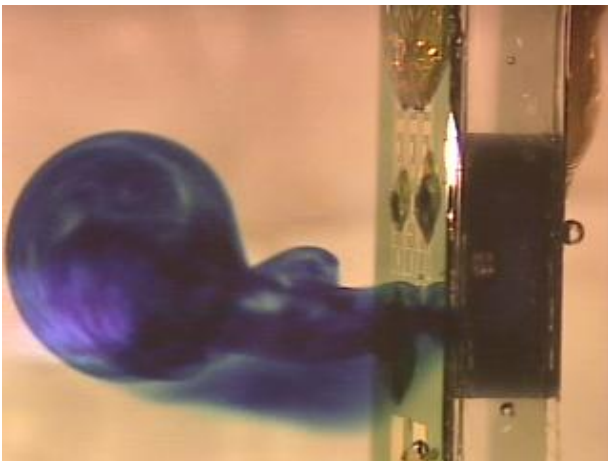


Figure 6: Side view of device showing release of methylene blue into a solution upon activation.

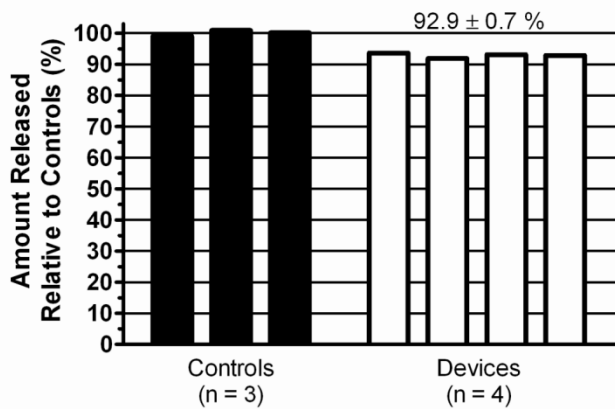


Figure 7: Quantification of released vasopressin by radiolabeled species.

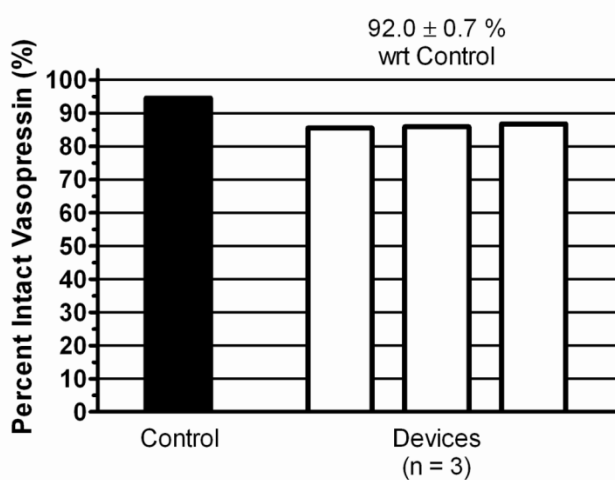


Figure 8: HPLC analysis of released vasopressin from IRD³.

Electronic Supplementary Material

1. Finite Element Analysis (FEA)

FEA analysis was performed on the membranes using Cosmos Works (Cosmos, Solidworks, Inc., USA). The structure was defined as 400 μm x 400 μm silicon nitride membrane with a 200 nm thickness. The boundary conditions were defined as fixed ends preventing displacement or moments. The stresses were simulated using the Von Mises method and the theoretical maximum tensile stress of amorphous silicon nitride (200 MPa), and meshed with 3×10^5 elements. Successive differential pressure values were simulated across the surface area of the structure while the resultant minimum safety factor (MSF) was subsequently monitored. The MSF is defined as the ratio of the breaking stress of a structure to the estimated maximum stress. Figure ESM.I shows the simulated structure with a factor of safety of 1.3 after a differential pressure of 5 kPa was applied. Figure ESM.II shows the stress distribution on the structure. Figure ESM.III and ESM.IV show the maximum strain and displacement distributions, respectively.

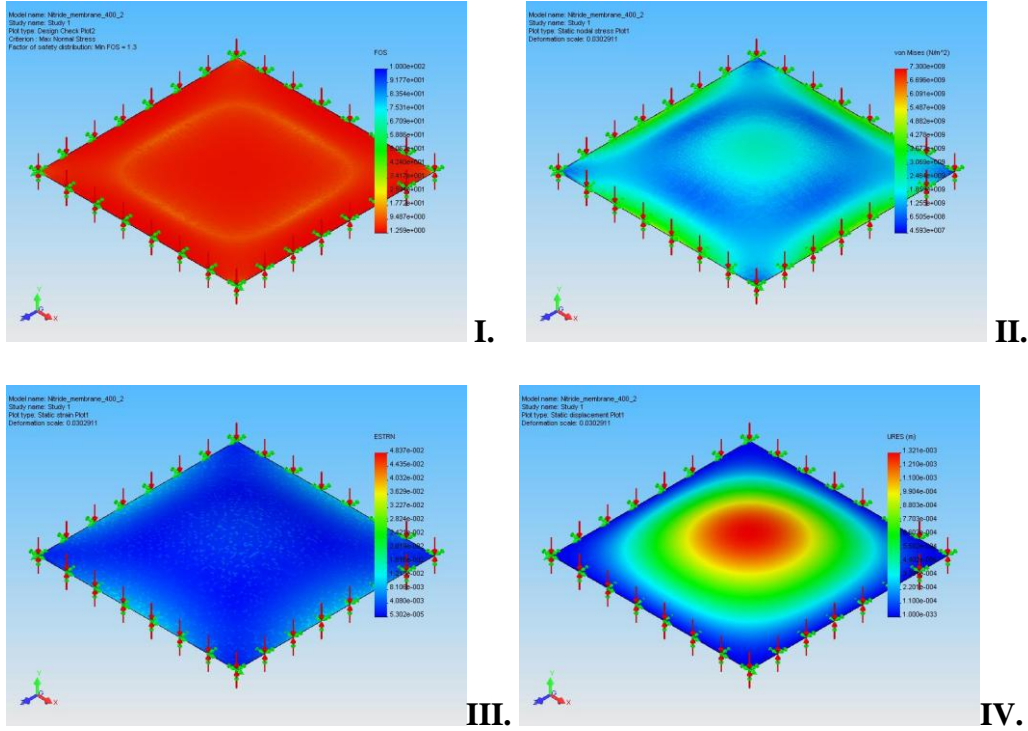


Figure ESM I,II, III, IV: Finite Element Analysis (FEA) simulation results.

2. Fabrication Process

The membrane layer was fabricated using micro-machining technology. A 500-nm thermal silicon dioxide (SiO_2) layer is grown on a 100-mm, double polished, 300- μm thick, single-crystal-silicon (SCS) wafer, followed by deposition of a 200-nm layer of SiN by low-pressure vapor chemical deposition (LPCVD). A 30-nm titanium adhesion layer and a 300-nm gold layer are then sputter-deposited. The first photolithographic step then defines the electrical fuses on top of the membranes. Gold and titanium are wet etched to form the fuses, shown in Fig. 2A. The patterned wafer is then coated with a layer of photoresist for protection. The backside of the wafer is photolithographically patterned to define the silicon nitride membranes. CF_4 -based reactive ion etching (RIE) first transfers the pattern to the backside SiN and SiO_2 layers, then deep RIE based on the

BoschTM process is performed to anisotropically etch through the wafer up to the front-side buried SiO₂ layer, shown in Fig. 2B. This layer acts as a stop mask, and allows compensation for approximately 10 percent etch non-uniformity commonly seen in the deep RIE processes (Elman, et al. 2008). The wafer is finally dipped in 49% HF for 2 minutes to remove the remaining oxide and release the silicon nitride membranes. The wafers are then diced into 5 mm x 5 mm chips.

The actuation layer was also fabricated using micro-machining technology on 100-mm SCS substrates. The process sequence is shown in Figure 3. The first step is to grow a 500-nm thermal SiO₂ layer, which serves to electrically isolate the substrate. Next, a 250-nm Ti layer followed by a 300-nm Au layer are sputtered, shown in Fig. 3A. The first photolithographic process is implemented to pattern Au electrical contacts, and is followed by an Au etch and Ti Etch, which defines the electrode layer, shown in Fig. 3B. The next steps are designed to encapsulate the resistors for protection against subsequent etch steps, and provide a robust adhesion layer for subsequent oxide deposition. Sputtering of 300 nm of Au and 20 nm of Ti is followed by the second photolithographic step. Ti and Au layers are then wet-etched sequentially to fully define the encapsulation of the resistors, Fig. 3C. The next step is to conformally deposit 2 μm of SiO₂ to isolate the electrodes layers, preventing electrolysis between electrodes from taking place once the device is fully packaged and operating, Fig. 3D. The third photolithographic step is implemented to define vias for bonding pads in the electrodes, and open areas in the resistors. A CF₄-based RIE is used to etch SiO₂ and the Ti adhesion layer to expose the bonding pads and the resistors. The last photolithographic step masks the bonding pads. This step is followed by an Au etch, finally exposing the Ti resistors.

The wafer is diced into 5 mm x 9 mm chips. The reservoir layer was defined using 100 mm, double polished, 2.25 mm thick Pyrex 7740 wafers. These wafers were drilled using a 1.7 mm radius diamond bit to achieve a reservoir volume of 20 μ l, and diced in 6 mm x 8 mm chips.

All three layers were bonded together using a biocompatible UV-cured epoxy (1-20542 cationic epoxy, Dymax Corporation, USA). The layers can also be anodically bonded for permanent hermeticity. The chips were filled by breaking one of the nitride membranes and dispensing solutions with known drug concentration through the opening using a 100 μ L syringe with a 32 Gauge needle (Hamilton Company, Reno, NV), mounted in an injection system consisting of a UMP-1 Ultra Micro Pump with Micro-1 controller and a Kite-R micromanipulator with a TB-1 tilting base (all from World Precision Instruments, Sarasota, FL). This system allows precise control of the amount of solution injected into the device, and by extension, the amount of loaded drug. The open membrane was subsequently sealed with UV-cured epoxy. Electrical cables and connectors were connected to the chip and wire-bonding was performed to connect the electrical wires to the chips. The final packaged device is shown in Fig. 4.

3. Release Characterization using Radiolabeled Vasopressin

The amount of volume released by the device was determined using a solution of arginine vasopressin (Sigma-Aldrich, Inc., USA) and ^3H -radiolabeled arginine vasopressin (American Radiolabeled Chemicals, Inc., USA). Four devices were filled with 20 μ L of radiolabeled solution following the procedure described above. An additional three controls were injected directly into water to be measured and determine

the loading in all devices. The test devices were activated for 45 seconds with an applied voltage of 9 V in 2 mL of DI water. The media was sampled immediately before and after each device activation. Media aliquots were measured in a liquid scintillation counter (Packard Tri-Carb 2200CA, Perkin-Elmer Life Sciences, USA) to determine the fraction of original loading that was released.

4. Release Characterization using HPLC Methods

Devices were activated as in the previous section in 5 mL of DI water and media samples were collected immediately after activation. Samples were analyzed by reverse-phase HPLC (RP-HPLC), using an Agilent 1200 Series with quaternary pump and a diode array detector (Agilent, Inc., USA). A gradient method was used in a Brownlee Spheri-ODS column (25 cm x 4.6 mm, 5 μ m, 100 Å, Alltech Associates, USA), with methanol and 0.1% trifluoroacetic acid (TFA) in water. The gradient used was 2 % TFA/min, starting at 0%. The flow rate was 1 mL/min and the detection wavelength was 220 nm. The Chemstation software (Agilent, Inc., USA) was used to measure the area under the observed retention peaks and calculate the area fraction of the vasopressin peak, which had a retention time of 16.8 minutes.